Fracture transmissivity as a function of normal and shear stress: first results in Opalinus Clay

Robert J. Cuss, Antoni Milodowski, and Jon F. Harrington

Transport Properties Research Laboratory, British Geological Survey, Keyworth, Nottingham, NG12 5GG, UK (rjcu@bgs.ac.uk)

Fracture transmissivity has been investigated along an idealised fracture for the influence of normal stress and for the transient behaviour during a slow shear experiment. A linear trend for the relationship between effective stress and transmissivity has been proposed for normal loads between 1 and 5 MPa; as effective stress increases transmissivity decreases. Transmissivity was very low throughout the complete spectrum of effective stresses examined and was close to the permeability for intact Opalinus Clay, suggesting that the fracture had effectively closed.

During active shearing at a constant normal load, fracture transmissivity was seen to initially reduce, probably due to clear smearing. A series of flux events were seen, with transmissivity increasing by a factor of four. Some of the flux events corresponded with dilation, whilst others did not. This suggests that the opening flow paths were localised and did not result in bulk dilatancy. During the course of the shear test the sample formed its own series of fractures and a complex pattern of deformation occurred along the fracture surface to a depth of less than 1 mm. The impression of the end of the injection hole clearly shows that the block underwent at least 5 mm of the total 6 mm of shear displacement.

The injection of fluorescein showed that flow along the fracture was not uniformly radial, as one might expect for such an experimental geometry. At the time of injection there were a number of dominant flow features, mainly in the direction of shear and only perpendicular on one side of the fracture surface. Flow occurred along the original fracture surface as well as the newly formed shear surface, indicating multiple pathways in a complex manner.

The evolution of fracture transmissivity is very complex, even along initially planar surfaces. Fracture transmissivity has been seen to be a function of normal stress and porewater pressure, and has also been seen to be a dynamic feature during shear.

Introduction

The evolution of permeability in rocks under hydrostatic stress conditions has been widely reported. Many researchers have shown that the permeability of shale decreases with externally applied stress (Dewhurst *et al*., 1999a; Dewhurst *et al*., 1999b; Katsube, 2000; Katsube *et al*., 1996a; Katsube *et al*., 1998; Kwon *et al*., 2001; Neuzil *et al*., 1984) and decreased porosity (Dewhurst *et al*., 1998; Schloemer and Kloss, 1997). A range of non-linear relationships have been proposed between permeability, porosity, and pressure in shale and mudstones, including exponential and power laws (Dewhurst *et al*., 1999a; Katsube *et al*., 1991).

Gutierrez *et al.* (2000) investigated experimentally the hydromechanical behaviour of an extensional fracture in Kimmeridge Shale under normal and shear loading. It was shown that, at the time it was created, the fracture probably had about nine orders of magnitude higher permeability than the current permeability of the intact shale. Increasing the contact normal stress across the fracture reduced the fracture permeability following an empirical exponential law. However, loading the sample to an effective normal stress twice as much as the intact rock unconfined compressive strength did not completely close the fracture, although it did reduce the permeability by an order of magnitude.

Shearing of the fracture at a constant effective normal stress lower than the unconfined compressive strength of the shale caused dilation of the fracture and an order of magnitude increase in fracture permeability. Shearing at a constant normal stress higher than the unconfined

compressive strength of the intact shale caused dilation of the fracture and about six orders of magnitude reduction in fracture permeability. The reduced permeability is due to shear-induced gouge formation and transported particles blocking the fracture apertures. However, despite the reduction being close to six orders of magnitude, the fracture permeability was still about three orders of magnitude larger the intact rock permeability.

The ability of rough fractures to retain much of their permeability in the presence of contact stresses across the fracture plane can be attributed to the microscopic structure and roughness of the fracture surfaces. Even in the case of severe loading exceeding the strength of the sediment matrix, it appears that the microscopic asperities at the fracture surface are able to keep open some space and channels along the fracture to allow for fluid flow and to maintain enhanced permeability.

EDZ related experiments at Mont Terri and in other underground rock laboratories are fundamental to our understanding of the stress-dependent response of permeability in argillaceous rocks. A higher hydraulic conductivity has been clearly observed in the excavation damaged zone (EDZ), where an interconnected and heterogeneous network of artificial fractures exists. In the rock zone immediately around the tunnel wall, permeabilities are orders of magnitudes higher than those in the undisturbed matrix further away from the tunnel (Blümling *et al.*, 2007).

The load plate experiment at Mont Terri (Buehler *et al.*, 2003) clearly demonstrated that the transmissivity of fractures formed around the EDZ is sensitive to loading. Generally, the transmissivity decreased with increasing load pressures, by up to a factor of 60. The decrease in flow follows the stepwise increase of the load pressure and is not being created by any other effect. However, it should be noted that even the reduced transmissivity observed at the highest load is still at least one order of magnitude greater than that of intact Opalinus Clay.

Experimental geometry

The Opalinus Clay is a Jurassic (Aalenian) marine clayshale. The formation, named after the ammonite Leioceras opalinum, consists of indurated dark grey micaceous claystones (shales) that are subdivided into several lithostratigraphic units. Some of them contain thin sandy lenses, limestone concretions, or siderite nodules. The clay-mineral content ranges from 40 – 80 wt % (9 – 29 % illite, 3 – 10 % chlorite, 6 – 20 % kaolinite, and 4 – 12 % illite/smectite mixed layers in the ratio 70/30). Other minerals are quartz (15 – 30 %), calcite (6 – 40 %), siderite (2 – 3 %), ankerite (0 – 3 %), feldspars (1 – 7 %), pyrite (1 – 3 %), and organic carbon (<1 %). The total water content ranges from 4 – 19 % (Gautschi, 2001).

Two 60 × 60 × 21 mm blocks of Opalinus Clay were prepared on a diamond mill. This gave smooth and parallel surfaces on both contact faces of the sample. The two blocks of material were measured and weighed prior to assembly of the apparatus; results are shown in Table 1. Moisture content was not measured for the test material, so in absence of this data it was taken from Horseman *et al.* (2007). Porosity, bulk density, dry density and degree of saturation were based on a measured grain density (BS1377: Part 2: 1990) of 2.69 $Mg.m^{-3}$. This shows that the sample was not saturated fully.

Apparatus

The direct shear rig is bespoke experimental apparatus designed for this study. It comprises 5 main components:

- Rigid frame that has been designed to deform as little as possible during the experiment;
- Normal load system comprising a rigid loading beam with 100× amplification of load, a rigid loading frame and a normal load thrust block allowing up to 10 MPa normal stress (36 kN force) on a sample 60 mm × 60 mm;

- Shear force actuator (comprising an ISCO 500 series D syringe pump) designed to drive shear as slow as 14 microns a day (equivalent to 1 mm in 69 days) at a constant rate along a low friction bearing;
- Pore pressure system comprising an ISCO 500 series D syringe pump that can deliver either water or gas through the centre of the top sample directly to the fracture surface;
- Data acquisition system using National Instruments LabVIEW™ software facilitating the remote monitoring and control of all experimental parameters.

The upper sample had a 4 mm hole drilled through the centre using a diamond drill. The top block of the sample assembly included a pore pressure injection pipe the same length as the thickness of the sample so that the filter at the end of the pipe was flush with the inner face of the sample block.

The two samples were located into brass blocks and held securely using bolts. The bottom sample is the one that is actively sheared. The top sample is sealed against the top thrust block by means of Mastic silicone sealant. This block is rigidly connected to the shear load cell which passes through the shear box through a seal, allowing the box to be filled with water. The top block is connected to the pore pressure delivery system and the normal load beam is then positioned to apply a uniform normal load. Sample dilation is measured by a high precision non-contact capacitance displacement transducer, which has a full range of ± 0.5 mm and an accuracy of 0.06 µm. A schematic of the experimental rig is shown in Figure 1.

Calculation of fracture transmissivity

Fracture transmissivity is calculated assuming radial flow from the injection hole given the steady state fluid flow rate Q and the pressure head H at the injection point. Steady flow in a cylindrical geometry is given by:

$$Q = \frac{2\pi T\left(h_i - h_0\right)}{\ln\left(r_o\right) - \ln\left(r_i\right)}$$

where T is the transmissivity, h_i is the head on the inner surface with radius r_i, and h_o is the head on the outer surface at radius r_o (Gutierrez *et al.*, 2000). For the experimental setup r_0 = 30 mm, r_i = 1.96 mm, h_0 = 0.05 m and h_i ~ 100 m, transmissivity (m^2/s) can simply be calculated from:

$$T = 1.183 \times 10^{-12} \frac{Q}{P_p}$$

if the fluid flux (Q in µl/hr) and pore pressure (P_p in kPa) are known. This relationship was used to calculate the transmissivity of the fracture throughout the experiment. A correction could be made for the change in contact area between the blocks, and hence the outer radius of the fracture, however scoping calculations showed this had only a negligible effect on the overall calculation compared with the uncertainty of how the fracture contact area changed with time.

Experimental programme

The experimental programme was designed to answer two specific questions:

- *Change in fracture transmissivity with normal load.* The current experimental programme included a phase of testing whereby normal load was increased or decreased on the two samples of Opalinus Clay and the flux along the idealised fracture was monitored. The samples undergo considerable swelling and each stage was held until steady-state flow was achieved; or near steady-state flow conditions if time did not permit. An additional test was conducted to investigate the role of pore pressure on the fracture transmissivity at increased porewater pressure.
- *Change in fracture transmissivity during active shear at a constant normal load.* For the main phase of the experiment the sample was held at a constant normal load and the two

blocks of Opalinus Clay were slowly sheared and the flux along the fracture surface was monitored. The injection pressure was held constant throughout the course of the experiment.

Fracture transmissivity variation with normal load

The aim of this part of the experiment was to investigate the effect of normal load on fracture transmissivity and also the effect of variable porewater pressure. The experimental programme included five different normal loads and a stage at an elevated pore pressure. The length of each test stage was between 2 and 6 days in order to attain quasi steady-state conditions. In total, part one of the test history lasted 29 days.

Figure 2 shows that during the full duration of the experiment a net dilation of 700 microns was observed. This is significant considering that the thickness of the two samples was 41.44 mm at the beginning of the experiment, equating to an axial strain of 1.7 % (lateral strain is not recorded). Maximum swelling was over 750 microns. As can be seen, each normal load step change results in dilation (swelling) of the sample. Initially the sample was loaded to 3 MPa normal stress, which rose to nearly 5.5 MPa as the result of 300 microns of sample swelling. The amount of swelling seen can be explained by the starting saturation of 81.4 % for the sample. At this saturation the samples would have been in a high degree of suction, resulting in considerable swelling of the clay material.

Fracture transmissivity was measured for 6 test stages (Table 2), one of which was at an elevated pore pressure of 2 MPa. As shown in Figure 3, a clear relationship between effective stress and transmissivity is observed. This suggests that transmissivity is inversely proportional to effective stress, as expected. The exact nature of the relationship isn't obvious as a logarithmic relationship also gives a good fit to the data. It should be noted that the transmissivity is very low throughout the complete spectrum of effective stresses and is close to the transmissivity for intact Opalinus Clay. The data suggests that the fracture is effectively closed at all effective stresses and is not contributing significantly to the observed permeability. It would appear that S1.8 is the furthest from the linear relationship of fracture transmissivity versus effective stress; this may be the result of hysteresis. The stages for decreasing normal load (S1.2, S1.5, S1.6 and S1.7) all follow the linear trend, whereas increasing the normal load from 2.5 MPa to 2.75 MPa for stage S1.8 has resulted in a greater reduction in transmissivity.

Figure 3 includes the step at elevated pore pressure, which does not correspond well with the rest of the data. One possible error in the position of this data point is the assumption of the effective stress law. However, if pore pressure distribution is uneven and the effective stress experienced by the fracture surface is likely to be greater due to a lower average pore pressure across the fracture surface; this would in fact make the relationship worse. It is more likely that this feature is the result of differences between the pore and matrix compressibility. Horseman *et al.* (2007) showed that a change in pore-water pressure at fixed total stress has a significantly larger effect on specimen volume than does a change in total stress at fixed pore-water pressure. Therefore it can be concluded that fracture transmissivity is not only a function of normal stress, it is a function of pore pressure. The effect should be corrected by the equation for calculating fracture transmissivity, but the difference in compressibility of pore and matrix is not included in the equation and is thus a factor in Opalinus Clay.

The investigation of fracture transmissivity with normal load was not the primary focus of the experimental programme. It has shown that fracture transmissivity is low and comparable with the permeability of intact Opalinus Clay. This shows that the closure of the artificial fracture has been very effective at the full range of normal stresses tested which corresponds to the results from Harrington *et al.* (2007) who observed a significant increase in permeability at effective stresses lower than around 1.0 MPa. The transmissivity of the idealised fracture is significantly lower than those seen in the Selfrac project (Trick, 2003). This indicates that the full scale Selfrac setup is measuring fracture transmissivity of a number of fractures and that the relationship observed is the result of a number of fractures closing at different rates dependent on

their orientation to the local stress field. This may be a result of the rough characteristics of natural fractures compared to the clean surface of the artificial fracture used in this study.

Fracture transmissivity during shear

The main focus of the experimental programme was to investigate the changes in fracture transmissivity during active shear at a constant normal load and single strain rate; this began when shear was initiated on day 29. The samples were actively sheared for a total of 70 days, with the final 35 days of the stage conducted without shear.

Figure 4 shows the result for shear load, which increased rapidly and reached a peak value of approximately 430 kg by day 4.84 (~1.2 MPa shear stress). The load slowly decayed, reaching a value of approximately 280 kg at day 43 and then slowly started to increase until day 56. On this day the experiment experienced controller problems and the test was temporarily halted. In restarting the experiment the shear actuator was accidently backed off. This relieved almost all shear load from the fracture surface. The controller was quickly stopped preventing any damage to the sample. Upon restarting, shear stress increased at a rate similar to that observed in the first few days of the test and returned to a level comparable with that before the incident.

Following day 60, shear load began to decay though by day 65 this trend had reversed and shear load began to increase. The cause of this was not known and as the sample was approaching the maximum shear displacement of 6 mm it was decided to stop shear displacement. Following this, shear load slowly decayed linearly for the remainder of the experiment. This could be explained by creep along the fracture plane.

Figure 5 shows the result of dilation during the shear experiment. In the early stage of the test the sample began to compress up to the point of maximum shear stress, when dilation became the dominant mechanism. This peaked at around 3 microns on day 21 when compressive deformation took over once more, with the sample slowly accommodating almost 15 microns of compression by day 70 when shear was halted. For the remainder of the experiment the sample underwent a further 1 micron of compression.

Figure 6 shows the result for fracture transmissivity for the duration of the test stage. Initially it can be seen that as shear stress increased, transmissivity remained fairly static at similar level to that observed before shearing was initiated. Transmissivity only started to change once the shear stress approached its maximum, when a decrease in transmissivity was noted. The flux along the fracture remained at this level for over 20 days with the exception of a small short-term variation at day 10.3.

The first of a series of flux variations occurred at day 29.83, followed by a second at day 32.83. Both of these short term peaks occur on a longer term flux increase. This was followed by significant flux events at day 40.16 and 45.16, with transmissivity peaking and then slowly decaying. These events were followed by the major transmissivity change which started at day 51.52, where transmissivity trebled and peaked at day 56. From this time onwards, flux slowly decayed, with the addition of three smaller peaks superimposed on the back of the major event. Generally flux decreased slowly until the end of the experiment. No major change in flux gradient is seen when shear was ceased, suggesting that the decay in flux was not as the result of mechanical shear deformation along the fracture surface.

The range of fracture transmissivities recorded during Stage 1 of the experiment (no shear, changing normal load) is shown in Figure 6 clearly showing the significance of the changes in flux. Initially, the flux reduces to a similar level seen when normal load was at its highest level in Stage 1. The series of flux events then resulted in flux much greater than seen by the effect of altering normal load alone. It can also be seen that the resultant flux seen at the end of the experiment is within the range of transmissivities seen in Stage 1 of the experiment. This suggests that this range of transmissivities is the sealing level of the idealised fracture and that the increase in flux is a major event happening along the fracture plane.

Figure 7 shows the result for the first 15 days of the shear experiment, corresponding to a "standard" shear test. In the first day of the stage, the sample continued to swell. As soon as shear began the sample started to compact until the point of shear stress maximum, when it started to dilate. The consequence of this volumetric strain was that flux started to reduce at approximately day 4.05. In general flux reduced from a level of ~37 µl/hr to 32 µl/hr between day 4 and day 6. It can be seen that the sample started to compact at day 4.05, with a secondary event at day 4.51, during which time flux reduced. The shear stress peak was achieved at day 4.84, which was soon followed at day 4.92 by the onset of dilation and a short-term flux peak at day 5.04. Flux peaked at day 10.32, this feature initiates at day 10 and does not correspond with anything seen in dilation, normal stress or shear load. This clearly shows that this change in flux is a localised event that has not resulted in bulk volumetric strain of the entire sample. A dilation event can be seen to initiate at day 11.2 and this may correspond with a short-term reduction of flux. The data clearly demonstrate that some flux variations do not register any dilation, while some dilation events do not correspond with variations in flux, further supporting the observation that localised events within the sample can affect the bulk transmissivity of the system.

Post-testing petrographical observations

On completion of the experimental tests the lower and upper synthetic fracture surfaces of the Opalinus Clay were examined for evidence of the presence and distribution of the fluorescein tracer dye, which was introduced into the pore fluid 63 days into the shear stage. Morphological features on the two shear surfaces were also characterised.

On opening the shear cell, the two counterpart sheared surfaces of the upper and lower clay blocks were immediately photographed before the surfaces of the clay blocks could dry out. The camera was mounted on a rigid photographic stand fitted with four quartz-halogen lamps providing incident illumination, the angle of which could be adjusted to give the desired illumination and shadowing as required. The surfaces were then re-photographed under both long (365 nm) and short (254 nm) ultraviolet (UV) illumination to reveal the distribution of fluorescein dye on the sheared clay surfaces.

The sheared clay surfaces were also photographed as stereo pairs in order to examine the morphological features across the whole sample surface. Stereo-pair photographs were examined using a mirror stereoscope to observe the morphology of the shear surfaces. The position and outline of morphological features such as ridges, troughs or valleys, and fractures were traced onto the photographs while observing the photographs under the stereoscope, to produce a detailed map of the surface morphology.

Laser-stimulated scanning fluorescence imaging (LSSFI) was performed using an Amersham Biosciences STORM™ 860 variable mode laser scanning system. This LSSFI scanning system was equipped with both red (635 nm) and blue (450 nm) laser diodes for red- and blue-excited fluorescence, with long-pass filters to allow recording of fluorescence emissions with wavelengths >650 nm and >520 nm, respectively.

Morphological characteristics of the contacting sheared clay surfaces

On opening the shear cell at the end of the experiment it was apparent that there was some bonding of the two clay blocks across part of their contacting area, and this necessitated the surfaces to be carefully prized apart in order to separate the blocks. The area where the two surfaces had bound together was seen to be disturbed on both blocks and occupied between about 25 – 30 % of the exposed surface of each block. The clay surface could be seen to be broken up and loose wedge-like fragments of clay had been pulled out of the surface. Tensional fractures orientated perpendicular to the direction of shear and parallel to the margin of the clay block were observed within this disturbed clay surface in the lower clay block only. Similar tensional features appear not to have formed in the surface of the upper clay block.

The relative displacement of the two clay blocks during shearing against each other was evident in the lower clay block surface from the position of the impression produced by the porous

sintered stainless-steel frit on the end of the fluid injection port tube. At the end of the experiment the final position of the frit on the lower clay surface was seen to have been displaced ~5 mm in the direction of shear.

Only about 20 – 30 % of the original flat, planar, contacting surfaces were visible on both the upper and lower clay blocks. Close examination of these surfaces revealed the presence of very faint, fine linear striations on both block surfaces. The striations were less than 0.1 mm wide and were orientated parallel to the direction of the shear movement.

A large proportion of the area of the exposed surface of each block appeared to be a new fracture surface created during the experiment. The two clay blocks parted largely by failure along this new fracture interface, leaving a thin selvedge of the upper clay block material "bonded" to the surface of the lower clay block. Detailed stereo photographic observations reveal that this surface is not a simple planar surface but is gently undulating, with a series of parallel or sub-parallel ridges and troughs that are orientated approximately perpendicular to the direction of shear or at an angle of between 45 – 60º to the direction of shear (e.g. Figure 8). The undulations or ridges have a typical spacing between 1 – 3 mm with amplitude estimated to be less than 0.1 mm. In some cases the surfaces of some troughs and ridges displayed evidence of polishing. This implies that some of these small irregularities may be shear surfaces, and could perhaps represent very small scale, anastomosing secondary or tertiary *Reidel-shears* developed in relation to shear movement along the original contacting clay surface. Observations from the stereo-photographs indicated the zone of deformation appears to have developed only in the upper clay block.

An impression left by the removal of the injection frit from the selvedge of upper clay block material reveals the presence of slickenside striations on the original shear plane. These striations are parallel to the direction of shear and indicate that there has been shear movement along the original shear plane between the upper and lower clay blocks. This would suggest that the fracture was formed relatively late in the shearing experiment.

A fracture orientated parallel to the shear movement direction cuts across the surfaces of both the upper and lower clay block just to the side of the injection frit, forming a marked step in the surfaces of both blocks (Figure 8). This fracture forms a prominent step up to 1 mm high in the surface of the two blocks. This step separates areas corresponding to the original planar clay contact surfaces from the new undulating clay contact surfaces of the thin selvedge of upper clay block. The height of this step suggests that the thickness of the zone of secondary Reidel shearing developed in parallel to the original contacting clay surface of the upper clay block is up to 1 mm wide. Laterally, this fracture terminates against the disrupted clay surface and against a region of deformed and sheared clay (Edge C in Figure 8). The stepped fracture comprises a series linked small dilational fractures or tension gashes developed and limited within the thin selvedge of upper clay block material. These form cross-joints or cross-fractures, linking the original shear plane between the two clay blocks and the new fracture defining the upper surface of the selvedge of upper clay block material. This region of deformed clay was only observed in the surface of the clay exposed in the trailing margin of the lower clay block and comprises a series of very closely-spaced, sub-parallel to anastomosing shear fractures, orientated parallel to sub-parallel to the block margin and perpendicular to the direction of shear movement. The fractures are imbricated and dip steeply towards the trailing margin of the block.

Distribution of the fluorescein tracer and fluid pathways

Fluorescein normally produces a strong green fluorescence emission colour under UV illumination. However, only a very weak fluorescence was observed from the contact surfaces from the upper and lower clay blocks. After enhancing the brightness and contrast in the digital photographs, weak luminescence could be observed from the clay surface. Much better images of the distribution of fluorescein on the contacting clay surfaces were obtained by LSSFI. This technique is very sensitive to very low levels of luminescence, and clearly revealed the distribution of the fluorescein tracer on the clay surfaces.

LSSFI and UV illumination observations revealed that the fluorescein was largely absent from much of the exposed areas of the original planar contacting shear surfaces in both the upper and lower clay blocks (e.g. Figure 8 and Figure 9). Only on the upper clay block, where the original clay contact surface came into contact with the zone of sheared clay in the lower clay block, did it display any presence of fluorescein tracer.

The selvedge of upper clay block material was removed carefully from the original shear plane surface of the lower clay block, and both contacting surfaces examined. The surfaces are both affected by slickenside striae. In addition, the impression of the injection frit in the lower clay block shear plane surface could be clearly seen to have migrated ~5 mm from its original position. Therefore, the late-stage fracture defining the upper surface of the selvedge of upper clay block material must have formed towards the end of the experiment.

LSSFI imaging of the bonded upper clay block selvedge showed that fluorescein tracer was only present over part of the shear surfaces: at the leading edge of the upper clay block and the trailing edge of the lower clay bock. This is adjacent to the zone of imbricate secondary shear fractures that was developed in the lower clay block. The fluorescein was observed to have spread laterally across the shear plane, away from the injection frit, in a direction broadly perpendicular to the direction of shear movement.

The fluorescein tracer was also seen to be present within a narrow ring in the clay immediately adjacent to the stainless steel frit on the end of the fluid injection tube (Figure 8 and Figure 9). It appears that the fluorescein has dispersed from this injection point in the following manner:

- Laterally along the pathways broadly delineated by the network of ridges and troughs on the gently undulating surface of the new fracture surface developed in the upper clay block. This new fracture surface is developed parallel and about 1 mm above the original clay contact surface. The flow-paths indicated by the fluorescein along this surface are broadly orientated perpendicular to the shear direction. It would appear that these troughs and ridges represent microscopic channels along which fluid could flow during the experiment.
- Locally along the original shear plane, at the leading edge of the upper clay block and the trailing edge of the lower clay block, along flow paths that are broadly perpendicular to the direction of shear.
- Laterally along the imbricate shear-fractures developed in the zone of deformed and sheared clay at the trailing edge of the lower clay block. These very fine and closely spaced shear fractures were conductive to fluid flow during the course of the experiment.
- Along the steep step fracture separating areas of original clay contact surface from the newly-generated fracture surface. This suggests that this fracture may have genuinely formed during the course of the experiment, and was not produced as an artefact during opening up of the shear cell.

A check was also made to look for evidence of fluid leakage along the interface between the clay and the fluid injection tube inserted into the upper clay block. No evidence for the presence of fluorescein could be found on the back surface of the upper clay block. Neither was any fluorescein detected around the hole left by the removal of the stainless-steel fluid injection tube. These observations strongly imply that there was a good seal between the clay and the walls of the fluid injection port, and that there is no evidence to suggest that pore fluid leaked along this interface.

A proposed mechanism for the development of flow paths in relation to the progress of shear experiment is illustrated in Figure 10, and is summarised below:

a) Initial flow of injected porewater moves along the original shear plane between the two clay blocks;

b) As shear progresses, the two opposing shear surfaces locally lock or bind at the leading edge of the upper clay block, initiating the formation of fine low-angle second-order shear fractures in the trailing edge lower clay block. Similar features were not observed in the upper clay block. The progression of shearing caused the imbrication of these fine second-order shear fractures, increasing permeability, with the result that porewater now flows through these new fracture features;

c) Formation and imbrication of second-order shear fractures continues until, near the end of the experiment, the opposing blocks bind locally, and any further movement is taken by a new fracture that forms within the upper clay block. This new fracture forms close to, and sub-parallel to the original shear plane. Movement along this fracture probably only started just prior to the end of the experiment, and hence the fracture surface shows only limited evidence of shearing. Porewater was able to flow along this new fracture in tensional asperities along the fracture surface, orientated perpendicular to the direction of shear movement.

Discussion

It has been observed that the two samples of Opalinus Clay have not undergone true self-healing along the fracture. This is common with the observations of the Selfrac project, which observed partial healing in Boom clay, but not in Opalinus Clay (Bastiaens *et al.*, 2007). During active shear the transmissivity data shows an initial reduction, which then evolved to a quasi steady state. The reduction in transmissivity created a flux along the fracture surface much lower than had been observed for elevated normal load (5.5 MPa as opposed to the 2.75 MPa of the shearing phase of experimentation). The reduction in flux is likely to stem from clay smearing along the fracture surface, which the current data shows is a more effective sealing mechanism than normal load alone.

During the first 4 days of shearing the sample underwent bulk compaction. This may have been in response to the increase in shear stress and/or the clay smearing and re-organisation of the clay packing along the shear surface. The sample began to yield at around day 5, just prior to the sample attaining maximum shear load. This event corresponds with the reduction in transmissivity and the start of sample bulk dilation. At peak stress, a flux pulse was observed, suggesting that a pathway was opened by the initiation of sliding, but that it was soon closed.

Post peak stress the sample underwent bulk dilation of approximately 2.5 microns between day 5 and day 15. During this period the flux remained constant. This suggests that the observed dilation was not as a result of new conductive pathways being opened. Therefore it is unlikely that this dilation is as a result of the new fracture being created, as the formation of the shear fracture so close to the injection port is likely to create enhanced fluid transfer.

The first flux events observed at day 29 and 32 may signify the formation of the zone of fine imbricate second order shears formed at the leading edge of the lower block. It is then possible that the flux and dilation events observed at day 40, 45, and 52, 53, and 54 relate to the formation of the late fracture surface. However, although the fracture began to form, it did not facilitate shear movement, with the majority of movement occurring along the polished artificial fracture surface. It should be noted that the flux increase that occurred on day 40 resulted in a greater transmissivity than observed during the investigation of the effect of normal load on a non-shearing fracture. This suggests that a new mechanism of fluid flow was operating and that the formation of a new pathway in the form of a fracture is a likely cause of such an increase. However, the dilation event seen at this time is small (~0.2 microns), which suggests that any deformation was localised and did not result in bulk dilation.

The formation of a new fracture surface caused the fracture transmissivity to greatly increase by a factor greater than four, reaching a peak at day 55. The reduction in fracture transmissivity during shear after the peak at day 58 suggests that the sample underwent self-sealing. This is likely to have occurred through the dilation of the shear surface, the formation of slicken lines

and swelling of the clay material near the fracture surface. Therefore it would suggest that as a flow path is opened, continued shear causes a petrophysical change either side of the fracture that results in the closure of the opening. However, it was noted that fracture transmissivity continued to reduce even when shearing was stopped at day 70 and no major dilation was recorded. It is possible that the water transmitted by the formed pathways resulted in localised swelling, slowly closing the pathways and reducing transmissivity.

It has been shown that the sample formed its own series of fractures and a complex pattern of deformation occurred along the fracture surface to a depth of less than 1 mm. It has been noted that the injection filter was no longer flush with the artificial fracture and that its new position corresponds with the upper surface of the newly formed fracture surface. This could possibly suggest that the new fracture was in some way influenced by the level of the injection filter. It is possible that fluid penetrated the upper block at the level of the injection frit at a point of weakness and that the penetration of the pore fluid resulted in the formation of the new fracture. There is no conclusive indication of where the new fracture initiated and it is also possible that the new shear surface formed due to some natural reason along a pre-existing plane of weakness.

The impression of the end of the injection hole clearly shows that the block underwent the full shear displacement, or at least 5 mm of the total 6 mm. At first it appears that the sample created its own fracture surface and that movement occurred along this surface, but this can be discounted due to the displacement of the hole in the upper block relative to the lower one. Therefore it is likely that the majority of displacement occurred along the clean fracture surface. There is evidence that a limited amount of movement occurred along the new fracture surface, but this is likely to be late in the deformation history. There are some slicken lines formed along the new surface, but these are not as well developed as elsewhere.

The injection of fluorescein towards the end of the shear displacement has shown that flow along the fracture was not uniformly radial, as one might expect for such an experimental geometry. At the time of injection there were a number of dominant flow features, with flow predominantly in the direction of shear and only perpendicular on one side of the fracture surface. It was also seen that flow occurred along the original fracture surface as well as the newly formed shear surface, indicating multiple pathways in a complex manner. Flow generally followed the path along the tensional step-feature observed towards the zone of shear fractures observed at the leading edge of the upper block.

The increase in shear stress observed between day 66 and day 70 could be the result of the locking of the selvedge of clay and the artificial fracture surface. This could have resulted in the new shear surface becoming the dominant failure plane, but that the two fracture planes resulted in an increase in shear stress. Had the experiment been continued it is possible that the new fracture surface may have become the dominant slip surface.

When shearing was stopped at day 70 the sample continued to reduce in fracture transmissivity. This suggests that the continued reduction in flux was not as the result of mechanical deformation and may have been as a result of swelling along the fluid pathways. However, shear load reduced during this period, which may suggest that slow creep deformation occurred along the transmitting fracture surface and that this resulted in some mechanically driven self sealing. It is noted that the final fracture transmissivity of the fracture returned to a value similar to that seen at the start of shearing, i.e. the pathway had almost self-sealed fully.

It is clear that the evolution of fracture transmissivity is very complex, even along initially planar surfaces. The exact timing of events is difficult to determine, but the description of events above is consistent with the observations made mechanically and petrographically.

Conclusions

A linear trend for the relationship between effective stress and transmissivity has been proposed for the 6 steps of normal load investigated between 1 and 5 MPa; as effective stress increases transmissivity decreases. The exact nature of the relationship remains uncertain though a

logarithmic relationship gives a good fit to the data. It should be noted that the transmissivity is very low throughout the complete spectrum of effective stresses examined and is close to the permeability for intact Opalinus Clay. This suggests that the fracture has effectively closed at all effective stresses and is not contributing significantly to the observed transmissivity. Considerable swelling was experienced by the sample, resulting in 700 μm of dilation, equating to 1.7 % axial strain.

A test was conducted to see the effect of pore pressure on the transmissivity of the fracture at 2 MPa pore pressure, the result was a flux over twice that for a pore pressure of 1 MPa. Therefore fracture transmissivity is not only a function of normal stress, it is a function of pore pressure and a change in pore-water pressure at fixed total stress has a significantly larger effect on specimen volume than does a change in total stress at fixed pore-water pressure. The effect should be corrected by the equation for calculating fracture transmissivity, but the difference in compressibility of pore and matrix is not accounted for and is thus a factor in Opalinus Clay.

Once shear was initiated, shear load increased rapidly and reached a peak value by day 4.84. The load slowly decayed, reaching a steady residual value by day 43 and then slowly started to increase until day 56. Shear stress began to rise around day 65 and this is likely to be as a result of the formation of a new fracture surface. A dilation event was noted at this time which corresponds with the increase in stress and is likely to be associated with the development of the new fracture plane.

In the early stage of the test the sample exhibited a general reduction in volume up to the point of maximum shear stress, when localised dilation became the dominant mechanism. This peaked at around 3 microns on day 21 when compressive deformation dominated. Fracture transmissivity remained approximately at the same level as before shearing was initiated and only started to change once the shear stress approached its maximum; reducing transmissivity. The reduction in flux is likely to stem from clay smearing along the fracture surface, which the current data shows is a more effective sealing mechanism than normal load alone. The flux along the fracture remained approximately at this level for over 20 days.

A series of longer-term flux events occurred; during these events flux along the fracture plane spontaneous changed, increasing or decreasing dependent on localised changes in fabric structure along the fracture plane. The final event resulted in a peak of transmissivity three times that seen earlier in the shear test. For the remainder of the experiment flux slowly decayed, the gradient of reduction did not change significantly when shear was stopped; suggesting that mechanical deformation along the fracture plane was no longer the dominant mechanism governing the evolution in transmissivity. The flux increase events were the result of new fracture formation. Some of this deformation was localised and did not register as a bulk dilatancy, while some fractures did show bulk dilatancy. As continued shear occurred some movement took place along the new surface and this deformation resulted in self-sealing and a reduction in transmissivity with time. Throughout the test a number of short term flux events were observed. Most of these were short lived (less than a day) and during the period of no shear were as short as 1 hour.

During the course of the shear test the sample formed its own series of fractures and a complex pattern of deformation occurred along the fracture surface to a depth of less than 1 mm. The injection filter was no longer flush with the artificial fracture and that its new position corresponds with the upper surface of the newly formed fracture surface. This could possibly suggest that the new fracture was influenced by the level of the injection filter, although there is no conclusive indication of where the new fracture initiated.

The impression of the end of the injection hole clearly shows that the block underwent the full shear displacement, or at least 5 mm of the total 6 mm of shear displacement. At first it appears that the sample created its own fracture surface and that movement occurred along this surface, but this can be discounted due to the displacement of the hole in the upper block relative to the

lower one. Therefore it is likely that the majority of displacement occurred along the artificial fracture surface. There is evidence that a limited amount of movement occurred along the new fracture, but this is likely to be late in the deformation history.

The injection of fluorescein towards the end of the shear displacement has shown that flow along the fracture was not uniformly radial, as one might expect for such an experimental geometry. At the time of injection there were a number of dominant flow features, with flow predominantly in the direction of shear and only perpendicular on one side of the fracture surface. Flow occurred along the original fracture surface as well as the newly formed shear surface, indicating multiple pathways in a complex manner. Flow generally followed the path along the observed tensional step-feature towards the zone of shear fractures at the leading edge of the upper block. The dismantling of the test sample showed that self-healing had not occurred and that the artificial fracture was intact and the dominant shear surface.

It is clear that the evolution of fracture transmissivity is very complex, even along initially planar surfaces. The exact timing of events is difficult to determine, but the description of events above is consistent with the observations made mechanically and petrographically.

Bastiaens, W., Bernier, F., and Li, X-L (2007) SELFRAC: Experiments and conclusions on fracturing, self-healing and self-sealing processes in clays. *Physics and Chemistry of the Earth* **32** pp. 600–615

Blümling, P., Bernier, F., Lebon, P., Martin, D. (2007): The excavation damaged zone in clay formations time dependent behaviour and influence on performance assessment. Physics and Cemistry of the Earth 32, Elsevier.

British Standard Methods (1990): Soils for civil engineering purposes, Part 2, BS 1377: Classification test, pp. 61.

Buehler, Ch., Heitz, D., Trick, Th. and Frieg, B. (2003) In-situ self-healing of the EDZ as a consequence of loading.Impact of the Excavation Disturbed or Damaged Zone (EDZ) on the performance of radioactive waste geological repositories: Proceedings of a European Commission CLUSTER conference held in Luxemburg on 3-5 November 2003, 231-236.

Dewhurst, D.N., Aplin, A.C., and Sarda, J.-P. (1999) Influence of clay fraction on pore-scale properties and hydraulic conductivity of experimentally compacted mudstones. *Journal of Geophysical Research*, **104**, pp. 29,261-29,274.

Dewhurst, D.N., Aplin, A.C., Sarda, J.-P., and Yang, Y. (1998) Compaction-driven evolution of porosity and permeability in natural mudstones: An experimental study. *Journal of Geophysical Research*, **103**, pp. 651-661.

Dewhurst, D.N., Yang, Y., and Aplin, A.C. (1999) Permeability and fluid flow in natural mudstones. In: Aplin, A.C., Fleet, A.J., and Macquaker, J.H.S., eds., *Mud and Mudstones: Physical and Fluid Flow Properties*, Geological Society of London, Special Publications, **158**, pp. 23-43.

Gautschi, A. (2001) Hydrogeology of a fractured shale (Opalinus Clay): Implications for deep geological disposal of radioactive wastes. *Hydrogeology Journal*, **9,** pp.97–107

Gutierrez, M., Øinob, L.E. and Nygardc, R. (2000) Stress-dependent permeability of a de-mineralised fracture in shale. *Marine and Petroleum Geology*, **17**, pp.895–907.

Horseman, S.T., Harrington, J.F., and Noy, D.J. (2007) Swelling and osmotic flow in a potential host rock. *Physics and Chemistry of the Earth* **32** pp.408-420

Katsube, T.J. (2000) Shale permeability and pore-structure evolution characteristics. *Geological Survey of Canada*. Ottawa, ON, Canada. Pages: 9.

Katsube, T.J., Boitnott, G.N., Lindsay, P.J., and Williamson, M. (1996) Pore structure evolution of compacting muds from the seafloor, offshore Nova Scotia. In: Anonymous, ed., Eastern Canada and national and general programs. *Current Research - Geological Survey of Canada*, pp. 17-26.

Katsube, T.J., Issler, D.R., and Coyner, K. (1996) Petrophysical characteristics of shale from the Beaufort-Mackenzie Basin, northern Canada; permeability, formation factor, and porosity versus pressure, Interior plains and Arctic Canada. *Current Research - Geological Survey of Canada*. pp. 45-50.

Katsube, T.J., Mudford, B.S., and Best, M.E. (1991) Petrophysical characteristics of shales from the Scotian shelf. *Geophysics*, **56**, pp.1681-1689.

Kwon, O., Kronenberg, A.K., Gangi, A.F., and Johnson, B. (2001) Permeability of Wilcox Shale and its effective pressure law. *Journal of Geophysical Research, B, Solid Earth and Planets*, **106**, pp. 19,339-19,353.

Neuzil, C.E., Bredehoeft, J.D. and Wolff, R.G. (1984) Leakage and fracture permeability in the Cretaceous shales confining the Dakota aquifer in South Dakota. In: *Proceedings of First C.V. Theis Conference on Geohydrology* in Dublin, Ohio. Jorgensen, D.G. and Signor, D.C. (eds.). National Water Well Association. pp.113-120.

Schloemer, S., and Krooss, B.M. (1997) Experimental characterisation of the hydrocarbon sealing efficiency of cap rocks. *Marine and Petroleum Geology*, **14**, pp. 565-580.

Trick, T. (2003) Selfrac Experiment: Hydraulic testing during the load plate test experiment (July 2002 to January 2003). *Technical Note* **TN 2003-15 1**, 14 February 2003.

Acknowledgements

The study was undertaken by staff of the Minerals and Waste Programme of the BGS using the experimental facilities of the Transport Properties Research Laboratory (TPRL). Co-funding for the study was provided by the Geosphere Containment research project of the BGS Science Budget and National Cooperative for the Disposal of Radioactive Waste (Nagra).

	Units	Top sample	Bottom sample
Average length	mm	59.6 ± 0.2	59.7 ± 0.1
Average width	mm	59.7 ± 0.1	59.6 ± 0.1
Average thickness	mm	20.6 ± 0.1	20.8 ± 0.1
Hole diameter	mm	3.92 ± 0.4	/
Volume	m^3	7.306×10^{-5}	7.41×10^{-5}
Average weight	g	175.8	176.9
Density	$g.cc^{-1}$	2.41	2.39
Combined volume	m^3	1.47×10^{-4}	
Combined Weight	g	352.7	
Density	$g.cc^{-1}$	2.40	
Grain density	$g.cc^{-1}$	2.69	
Moisture weight	g	20.5	
Moisture content	%	5.8	
Dry weight	g	332	
Dry density	$g.cc^{-1}$	2.26	
Void ratio		0.2	
Porosity	%	16	
Saturation	%	81	

Table 1 Dimensions and properties of the Opalinus clay test material based on a grain density for the mineral phases of 2690 $kg.m^{-3}$.

Stage	Effective stress (MPa)	Transmissivity (m^2/s)
1.2	4.62	4.22×10^{-14}
1.3#	3.74	4.7×10^{-14}
1.5	3.8	4.38×10^{-14}
1.6	2.57	4.56×10^{-14}
1.7	1.11	4.89×10^{-14}
1.8	1.74	4.59×10^{-14}

Table 2 Results of average fracture transmissivity for each constant pressure step. # denotes stage at elevated pore pressure.

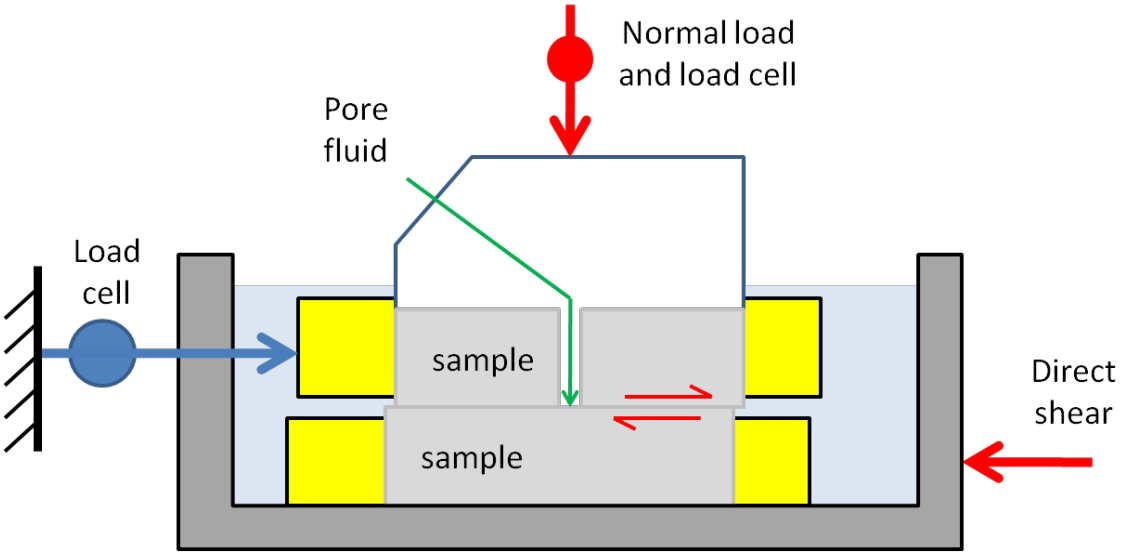

Figure 1 Schematic of the direct shear rig.

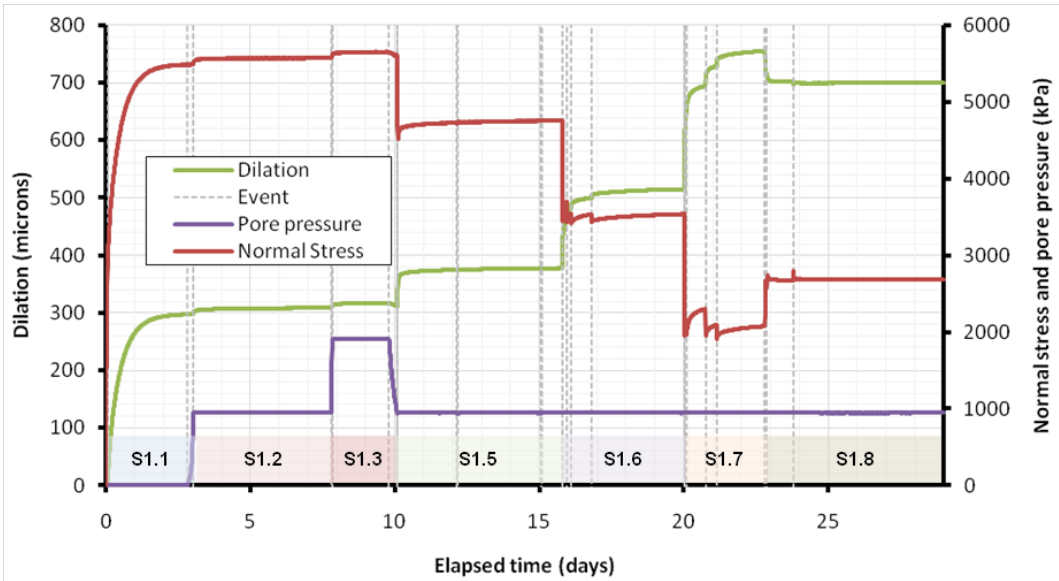

Figure 2 Dilation for Part 1 of the test history. Significant dilation occurs, particularly during the first days of the test when the sample swelled. Considerable swelling also occurs during each change in normal load.

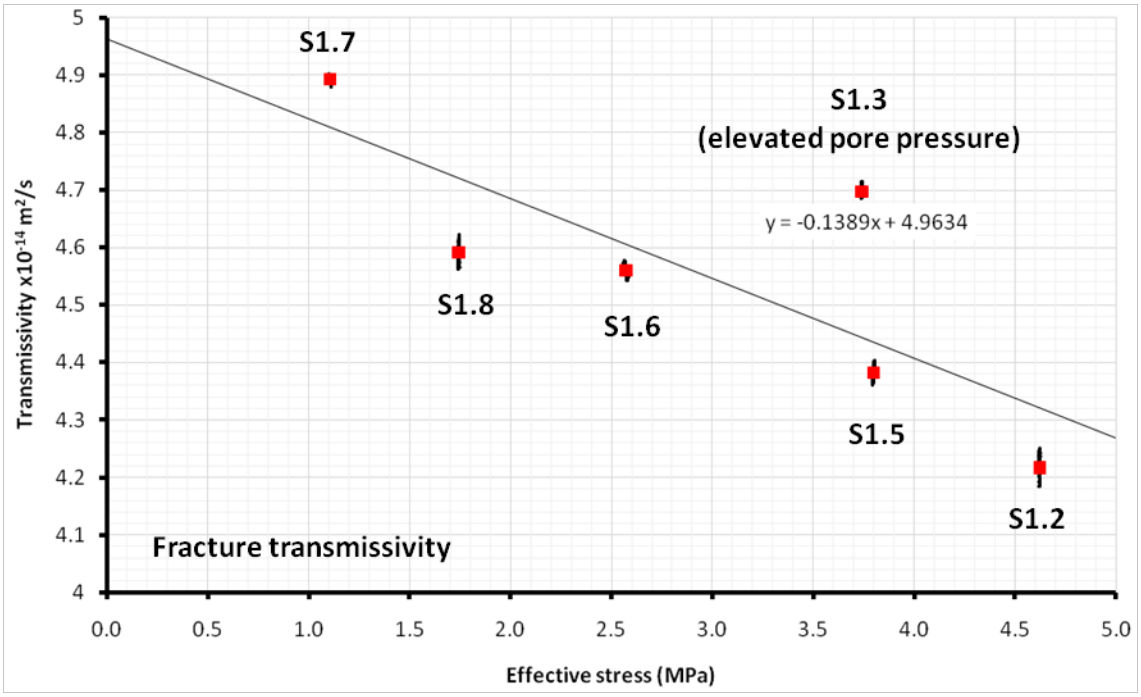

Figure 3 The relationship of fracture transmissivity versus effective stress including the stage at elevated pore pressure.

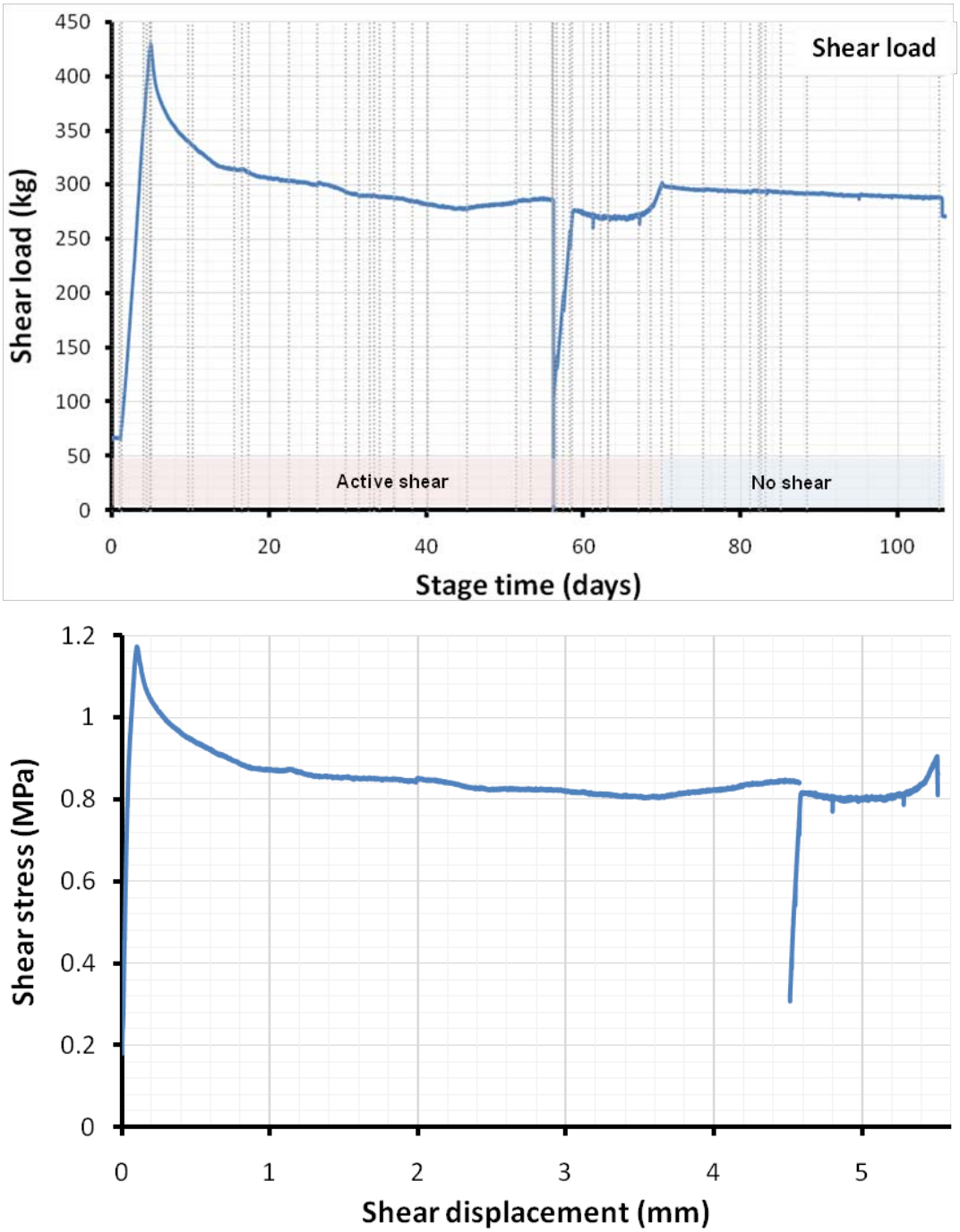

Figure 4 Shear stress/load during the constant displacement stage. The upper plot shows shear load versus time. The exact contact area between the upper and lower blocks is not known. However, shear stress (lower image) can be determined assuming stable movement along the fracture surface.

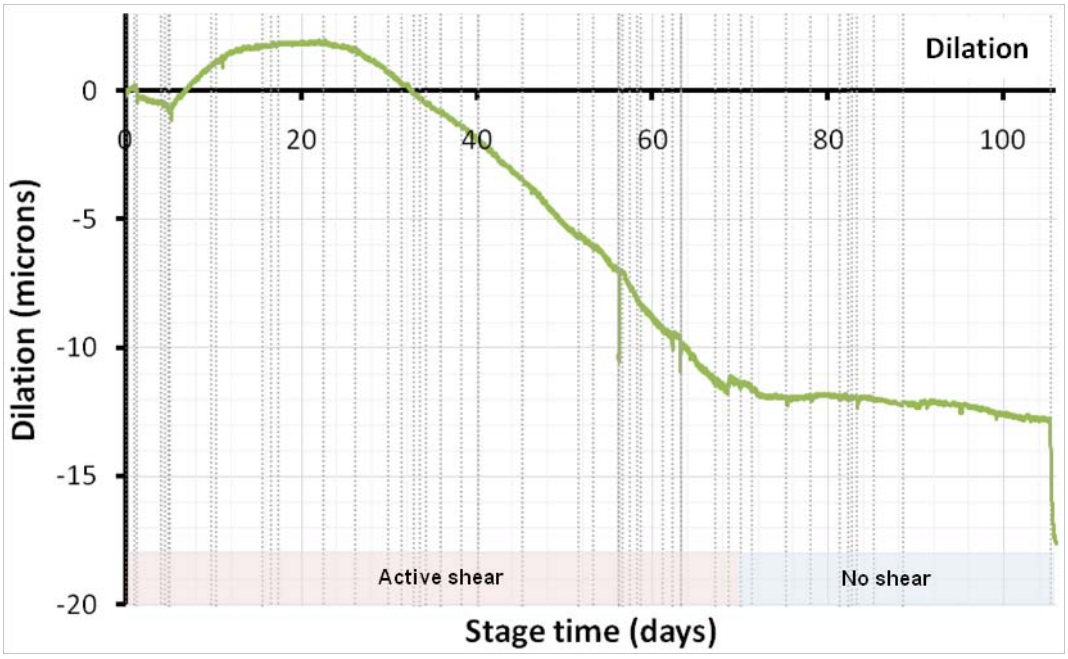

Figure 5 Plot of dilation during active shear.

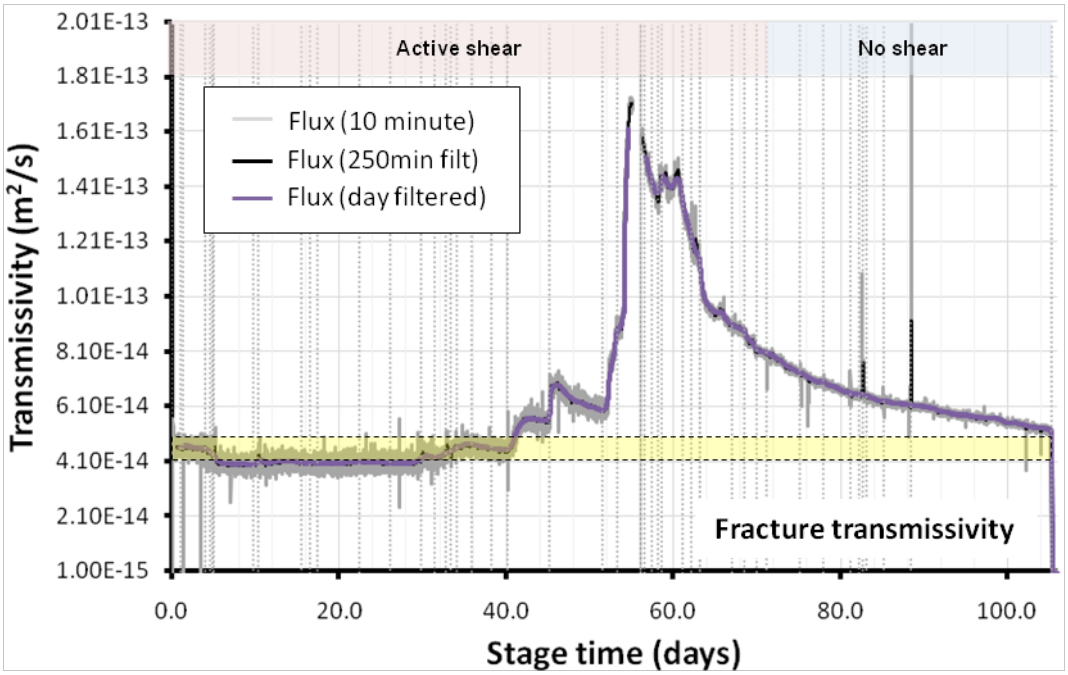

Figure 6 Fracture transmissivity during active shear. As seen, transmissivity is a dynamic property that alters during shear. The yellow band shows the range of fracture transmissivities recorded during Stage 1 of the experiment with no shear.

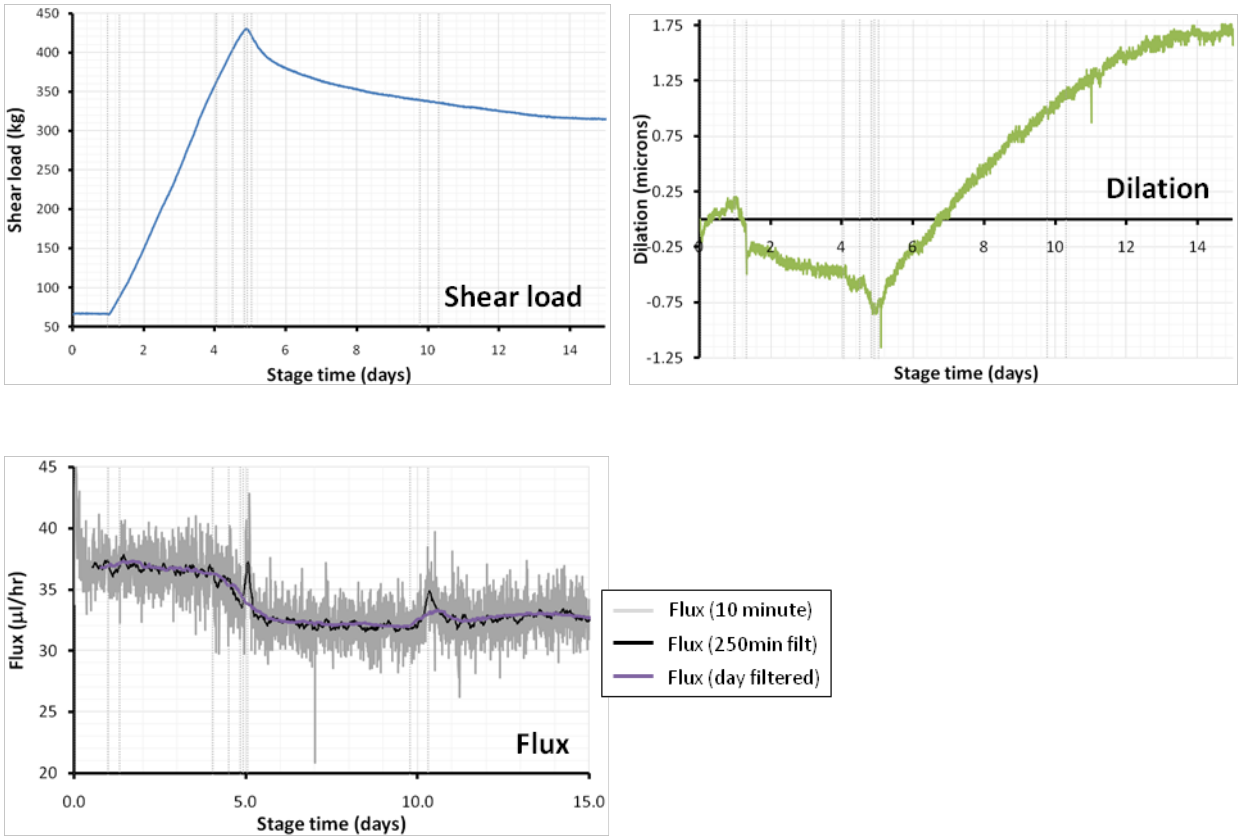

Figure 7 Data for the first 15 days of the shear experiment showing features in more detail.

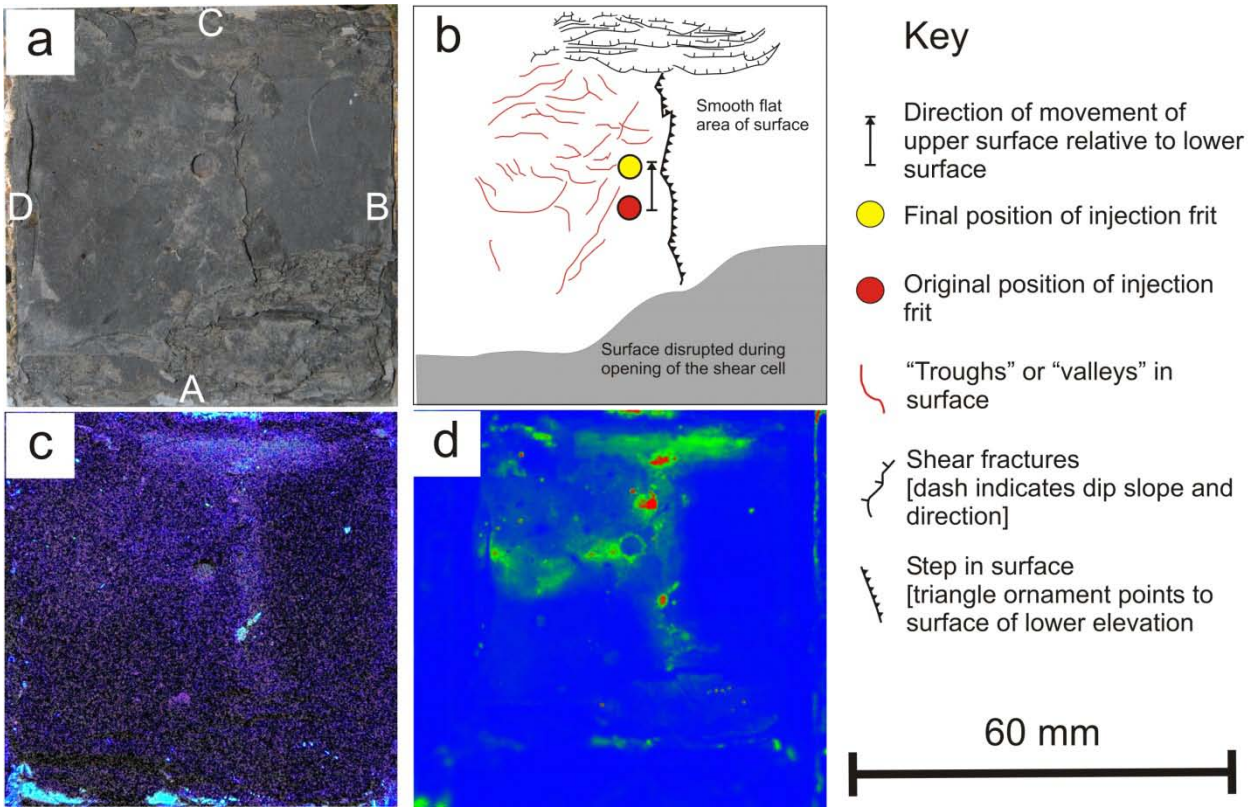

Figure 8 Morphology and distribution of fluorescein dye on the sheared surface of the lower Opalinus Clay block: (a) Normal visible light photograph showing circular impression produced by the porous frit from the fluid injection tube that penetrated through the upper clay block, showing its final position at the end of the experiment. The notation A, B, C, and D identifies the orientation of the clay block (shear towards C); (b) Traces of lineations and other morphological features defined from stereo photographs, corresponding to the same area as (a); (c) Photograph of the same area seen in (a) under near-ultraviolet illumination showing weak fluorescence from the fluorescein tracer dye across the surface of the lower clay block; (d) Laser-stimulated scanning fluorescence image (LSSFI) under blue (450 nm) excitation of the same area seen in (a) clearly showing the localised distribution of fluorescein tracer dye on the contact surface of the clay block. The relative concentration of the fluorescein is indicated by the rainbow colour scale [RED = high concentration; BLUE = absent].

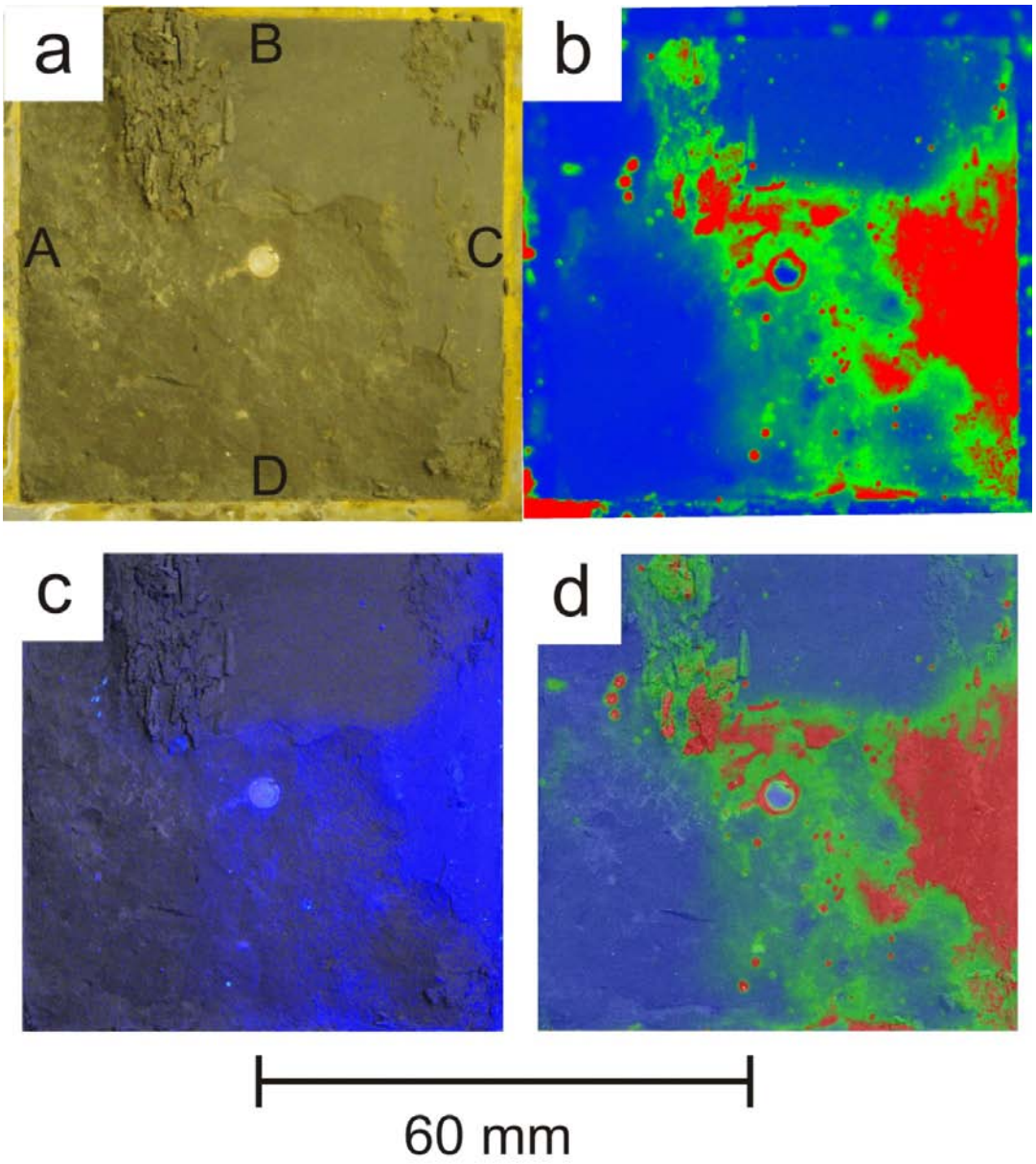

Figure 9 Distribution of fluorescein dye on the sheared surface of the upper Opalinus Clay block (a) Normal photograph of the post-experiment contact surface of the upper clay block. The smooth area in the top right hand corner of the clay surface is the original clay surface contact area. The rough area in the bottom half of the image is largely the new fracture surface created during the experiment (b) Laser-stimulated scanning fluorescence image (LSSFI) under blue (450 nm) excitation of the same area clearly showing the localised distribution of fluorescein tracer dye across the contact surface of the upper clay block. The relative concentration of the fluorescein is indicated by the rainbow colour scale [RED = high concentration; BLUE = absent]. (c) Short UV fluorescence image superimposed onto the photograph of the block surface. The blue fluorescence shows the distribution of fluorescein. (d) LSSFI image superimposed onto the photograph of the block surface.

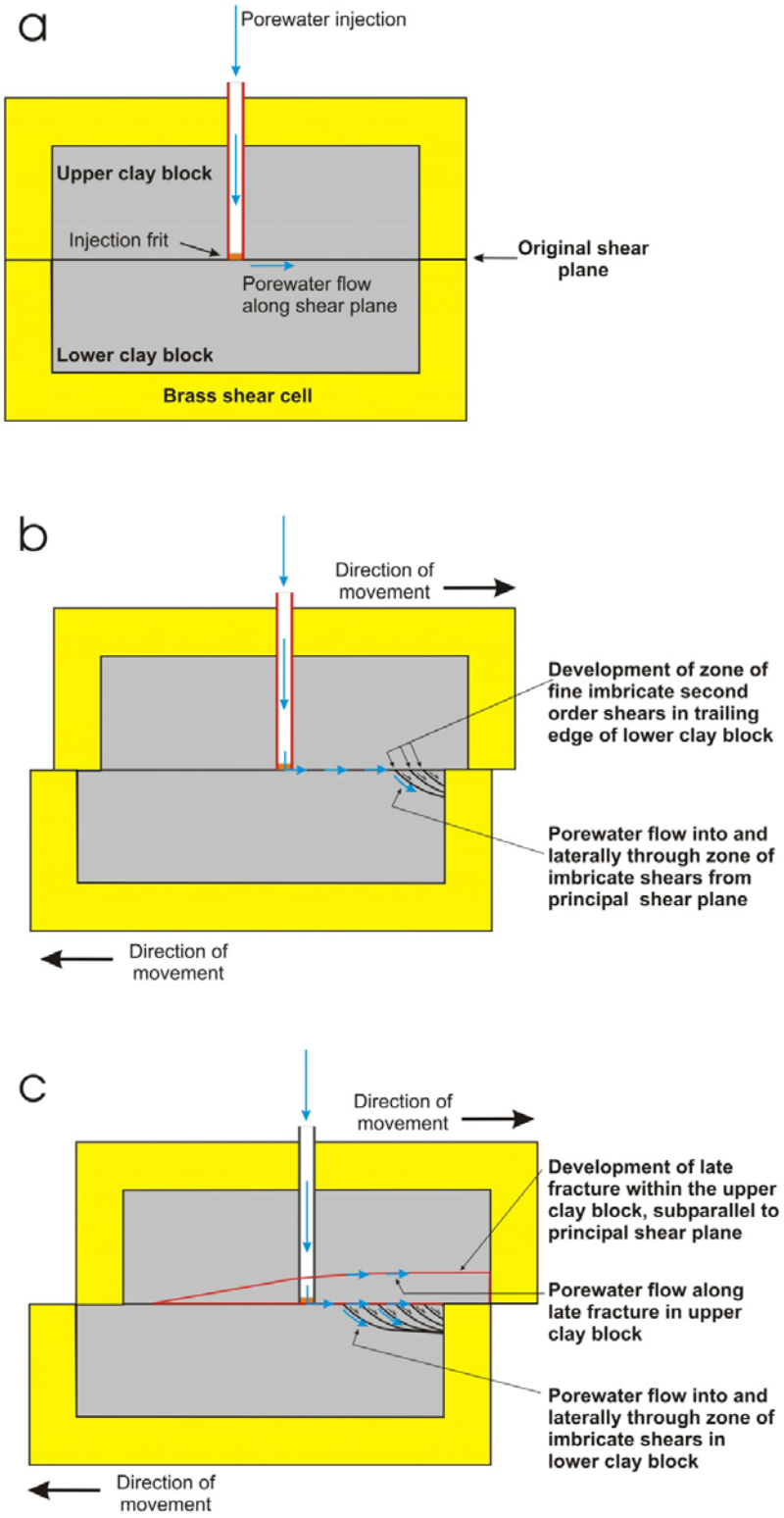

Figure 10 Simplified schematic model (not to scale) illustrating the development of secondary fracturing and porewater flow pathways (identified from fluorescein tracer observations) during the progress of the shear experiment.